Martian crustal dichotomy and Tharsis formation by partial melting coupled to early plume migration

Ondřej Šrámek[1] and Shijie Zhong[1]

Received 17 May 2011; revised 2 November 2011; accepted 3 November 2011; published 18 January 2012.

[1] A recently proposed model links the formation and early evolution of the Tharsis volcanic province on Mars to the preexisting hemispheric dichotomy (Zhong, 2009). A key aspect of this model is the assumption of a deep lithospheric root below the thicker crust of the southern highlands. We implemented a parameterization of partial melting into the 3-D spherical shell mantle convection code CitcomS in order to investigate whether the required lithospheric thickness variation can be generated self-consistently by partial melting when stiffening of the melt residue due to devolatilization is considered. The rate of melt production strongly depends on the mantle temperature, and additional strong coupling between the flow and partial melting is introduced through the stiffening effect on the melt residue. We find that it is possible to generate a lithospheric keel by partial melting above a single upwelling that excites a relative rotation between the one-plate lithosphere and the mantle below while producing the amount of melt distributed in a broad region constrained to one hemisphere that is necessary to form the crustal dichotomy. This scenario thus offers an internal mechanism for the Martian dichotomy formation and validates the hypothesis of Zhong (2009).

Citation: Šrámek, O., and S. Zhong (2012), Martian crustal dichotomy and Tharsis formation by partial melting coupled to early plume migration, *J. Geophys. Res.*, *117*, E01005, doi:10.1029/2011JE003867.

1. Introduction

[2] The crustal dichotomy and the Tharsis volcanic province are major global physiographic features on Mars. The dichotomy, clearly manifested as a mean elevation difference between the lower-topography northern and higher-topography southern hemispheres, was already identified from the Mariner 9 data [e.g., *Hartmann*, 1973]. It is well explained by a bimodal crustal thickness distribution [*Neumann et al.*, 2004]. The formation mechanism of the more ancient dichotomy (~4.1 Ga [e.g., *Nimmo and Tanaka*, 2005]) remains a subject of an extensive debate in planetary science. Different hypotheses invoke both external causes such as a giant impact [*Wilhelms and Squyres*, 1984; *Andrews-Hanna et al.*, 2008; *Marinova et al.*, 2008; *Nimmo et al.*, 2008; *Reese et al.*, 2010] or multiple impacts [*Frey and Schultz*, 1988], and mechanisms of internal dynamics such as long-wavelength mantle convection [*Lingenfelter and Schubert*, 1973; *Wise et al.*, 1979; *Zhong and Zuber*, 2001; *Roberts and Zhong*, 2006; *Ke and Solomatov*, 2006], a large-scale overturn of unstable postmagma ocean cumulates [*Elkins-Tanton et al.*, 2003, 2005] or an early episode of plate tectonics on Mars [*Sleep*, 1994; *Lenardic et al.*, 2004].

[3] Tharsis volcanic province in the western hemisphere is the location of most volcanism on Mars in the last ~4 Gyr [*Banerdt et al.*, 1992; *Tanaka et al.*, 1992]. The bulk of Tharsis was probably in place before the Late Noachian or one to few hundred Myr after dichotomy formation [*Phillips et al.*, 2001; *Solomon et al.*, 2005; *Nimmo and Tanaka*, 2005]. A mantle plume origin remains the most prevalent explanation for Tharsis [*Hartmann*, 1973; *Harder and Christensen*, 1996; *Breuer et al.*, 1996; *Kiefer*, 2003; *Solomon et al.*, 2005; *Roberts and Zhong*, 2006], even though an "edge-driven convection" was also proposed [*King and Redmond*, 2005]. Analyses of tectonic and volcanic features in the western hemisphere of Mars suggest a timed sequence of tectonic centers and an early migration of Tharsis volcanism from southern latitudes (~40°S) toward the equator over the first few 100 Myr of Tharsis existence [*Frey*, 1979; *Mège and Masson*, 1996; *Anderson et al.*, 2001; *Johnson and Phillips*, 2005]. Recently, on the basis of analyses of crater density and new geological mapping of the southern hemisphere, *Hynek et al.* [2011] suggest that the Tharsis volcanism may have started near the center of the southern highlands at even higher latitudes.

[4] The spatial characteristics of both the crustal dichotomy and the Tharsis province on a global scale (both are predominantly spherical harmonic degree 1 constructs), their present-day relative orientation (Tharsis straddles the dichotomy boundary), and the inferred early migration discussed above motivated *Zhong* [2009] to propose a dynamic model that links these two global scale structures. In this model, it is assumed that the dichotomy was generated by partial melting with a strong hemispheric asymmetry, as would be the case of melting above a single major upwelling in mantle convection with a spherical harmonic degree 1 planform [e.g., *Zhong and Zuber*, 2001; *Roberts and Zhong*,

[1]Department of Physics, University of Colorado at Boulder, Boulder, Colorado, USA.

0148-0227/12/2011JE003867

Table 1. Parameters of Convection Calculations

Parameter	Value	Unit
Planetary radius	3400	km
Core radius	1650	km
Gravitational acceleration	3.73	$m\ s^{-2}$
Mantle density	3400	$kg\ m^{-3}$
Thermal diffusivity at CMB	2×10^{-6}	$m^2\ s^{-1}$
Thermal diffusivity at surface	1×10^{-6}	$m^2\ s^{-1}$
Thermal expansivity at CMB	2×10^{-5}	K^{-1}
Thermal expansivity at surface	4×10^{-5}	K^{-1}
Specific heat at constant pressure	1200	$J\ K^{-1}\ kg^{-1}$
Surface temperature	220	K
Activation energy	157	$kJ\ mol^{-1}$
Activation volume	2.69	$cm^3\ mol^{-1}$
Rayleigh number	1.25×10^8	

2006]. Consequently, the thicker crust below the southern highlands is considered underlain by a thick lithospheric keel that represents a devolatilized residue after partial melting [*Pollack*, 1986; *Hirth and Kohlstedt*, 1996]. The lateral viscosity variations due to the keel could then excite a strong toroidal velocity flow field, including a degree 1 toroidal motion, i.e., a relative motion between the one-plate lithosphere and the underlying mantle.

[5] This hypothesis was tested using convection models with a prescribed lithospheric keel spanning one hemisphere (i.e., the hemisphere with thickened crust) [*Zhong*, 2009; *Šrámek and Zhong*, 2010]. The thermal upwelling of one-plume convection first forms below the thickest lithosphere at the center of the keel. Subsequently, a rotation between the lithosphere and the upwelling plume is observed, such that the upwelling migrates toward regions of smaller lithospheric thickness. When the upwelling reaches the keel edge (i.e., the dichotomy boundary), the relative motion ceases. The volcanism above the plume would show a pattern of early migration and subsequent stabilization near the dichotomy boundary, as inferred for Tharsis.

[6] However, our previous dynamic models did not include partial melting from the plume and formation process for the crustal dichotomy, which prevented us from addressing the question of whether the large lithospheric thickness variation can be self-consistently produced. Although previous studies [*Kiefer*, 2003; *Li and Kiefer*, 2007; *Ogawa and Yanagisawa*, 2011] considered partial melting in 2-D regional scale mantle dynamic models for Tharsis and Martian mantle convection in general, *Keller and Tackley* [2009] first investigated the possibility of dichotomy formation by partial melting in 3-D global mantle dynamic models. However, they focused on the production of the crustal material; devolatilization effects of partial melting were not considered, and therefore the modulation of the flow by the stiff melt residue could not be captured. Here, we newly include a consistent description of partial melting in our model. We consider the effect of partial melt residue stiffening on the plume-lithosphere dynamics to address the following questions: Can the lithospheric thickness variation with a strong hemispheric pattern (and a corresponding crustal thickness pattern) be generated as a result of partial melting? Is such a lithospheric thickness variation sufficient to excite the relative motion between the lithosphere and the mantle, as was the case with a prescribed lithospheric keel in our previous models [*Zhong*, 2009; *Šrámek and Zhong*, 2010]?

2. Model

[7] We investigate thermal convection in a 3-D spherical shell representing Martian mantle, following our previous studies [*Roberts and Zhong*, 2006; *Zhong*, 2009; *Šrámek and Zhong*, 2010]. The model setup is the same as that of *Šrámek and Zhong* [2010] and *Roberts and Zhong* [2006] except for the partial melting. The incompressible mantle under the extended Boussinesq approximation is heated both from within and from below. Viscosity $\eta(r, T)$ is depth and temperature dependent [*Roberts and Zhong*, 2006; *Šrámek and Zhong*, 2010], and includes a 25-fold increase in viscosity at 1020 km depth. It was shown that such a viscosity profile results in generation of a spherical harmonic degree 1 convection in a relatively short time ($\sim$100 million years) [*Roberts and Zhong*, 2006]. Possible mechanisms for such a viscosity increase with depth were discussed in previous studies [*Roberts and Zhong*, 2006; *Zhong and Zuber*, 2001], although significant uncertainties remain. The depth-dependent thermal conductivity $\alpha(r)$ and thermal diffusivity $\kappa(r)$ are linear functions of radius. The Rayleigh number Ra is calculated from the reference values of thermal expansivity, thermal diffusivity and viscosity at the bottom of the mantle, and uses the planetary radius as the characteristic length scale.

[8] The equations are solved using the finite element convection code CitcomS [*Zhong et al.*, 2000, 2008] with tracers for the compositional field [*McNamara and Zhong*, 2004]. Isothermal and free-slip boundary conditions on temperature and velocity are imposed on top and bottom boundaries. The parameters of the calculations are listed in Table 1.

[9] The main new aspect of the present model is the inclusion of partial melting which is discussed in detail here. We use the melting parameterization of *Katz et al.* [2003] and use tracers to monitor the degree of melting. At each time step after the new temperature field is calculated, we perform the following procedures that were added to the CitcomS code.

[10] 1. For each tracer position, we calculate the equilibrium degree of dry melting F_{eq} from the local (P, T) condition (given by *Katz et al.* [2003]) and compare it to the actual degree of melting F which is advected by the tracers.

[11] 2. If $F_{eq} > F$, the amount $F^{tr}_{new} = F_{eq} - F$ of new melt must be generated at the tracer and the degree of melting is updated ($F_{eq} \rightarrow F$). If $F_{eq} \leq F$, no new melt is generated ($F_{new} = 0$).

[12] 3. Then for each finite element, the degree of new melting F^{el}_{new} is calculated as the average value over the tracers (F^{tr}_{new}) within this element. The volume of newly generated melt in each element is readily computed. We assume a density of 2800 kg m^{-3} for the melt (i.e., crustal material), that is, a difference of 600 kg m^{-3} between the mantle and crustal densities.

[13] 4. The values of newly generated melt volume are then projected from the centers of elements to the nodal points.

[14] 5. We assume that the newly produced melt is immediately extracted to the surface where it increases the local crustal thickness above the subsurface melting location. Therefore, at each lateral nodal point location, we sum up the contributions from all the nodes along the vertical,

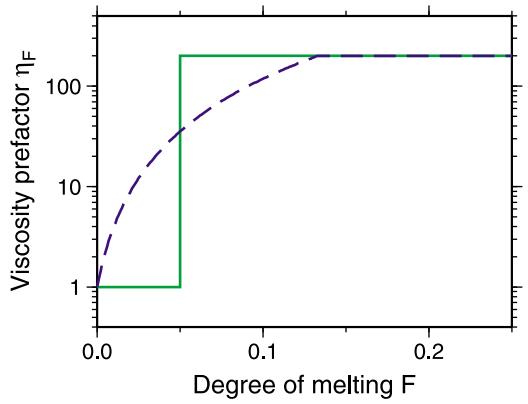

Figure 1. Compositional viscosity prefactor η_F as a function of degree of melting F. Step function (solid green line) and continuously varying η_F (dashed blue line).

and calculate the new addition to the crustal thickness at the corresponding surface nodal point. This is clearly a crude simplification that neglects the transport of partial melt in the upper mantle and crust, however, it is an obvious approximation in a global convection model, similar to previous studies [*Kiefer*, 2003; *Li and Kiefer*, 2007; *Keller and Tackley*, 2009].

[15] 6. A nonzero surface horizontal velocity (e.g., relative motion of lithosphere shell to the mantle) also requires advection of the crustal thickness field that is generated by the extracted partial melt.

[16] 7. The latent heat of melting is accounted for as a heat sink in the energy equation in the next time step. We use a value of 640 kJ kg^{-1} for the latent heat [*Navrotsky*, 1995].

[17] The presence of hydrogen (water) can decrease the solidus temperature significantly [e.g., *Kushiro et al.*, 1968]. Even though some argue for the mantle source region of recent volcanism on Mars to be relatively dry (<36 ppm [e.g., *Carr and Wänke*, 1992]), others suggest water concentration up to several hundred ppm (i.e., comparable to terrestrial mantle) [*McSween et al.*, 2001], and even higher water content for primordial mantle [*Médard and Grove*, 2006]. *Hauck and Phillips* [2002] argue that wet primordial mantle is required to satisfy the constraints on thermal and crustal evolution of Mars. In this study we only use the dry solidus of *Katz et al.* [2003]; it is very close to the *Bertka and Holloway* [1994] solidus that was used in several previous studies investigating Martian melting [e.g, *Kiefer*, 2003; *Li and Kiefer*, 2007], and slightly colder than the *Herzberg et al.* [2000] solidus used by *Keller and Tackley* [2009].

[18] The use of a melting relation for a nominally anhydrous mantle may seem to introduce an inconsistency into our model, given that we do consider the effect of dehydration on the melt residue. However, as *Hauck and Phillips* [2002] suggest, the effect of hydrogen on rheology is probably stronger than its modification of melting. Moreover, in our model, using a hydrous melting relation would have similar effect as increasing the mantle (i.e., CMB) temperature, which is varied in our models. In any case, detailed investigation of different melting parameterizations in not the focus of this study.

[19] The residual material left behind after melting is assumed to have increased viscosity due to devolatilization (dehydration) compared to mantle that has not been subject to partial melting. We have considered two different parameterizations of the melt residue viscosity prefactor η_F as a function of the degree of melting F. In some cases, we used a simple step function viscosity prefactor equal to 1 below and 200 above a 5% degree of melting threshold. It is also possible to treat hydrogen (water) as an incompatible trace element characterized by a distribution coefficient $D_H = X_H^{\text{solid}}/X_H^{\text{melt}}$ where X_H is the concentration of hydrogen; the usually adopted value is $D_H \approx 0.01$ [e.g., *Katz et al.*, 2003]. The viscosity variation with hydrogen content has been shown to follow $\eta \propto (X_H^{\text{solid}})^{-p}$ with $p \approx 2$ [e.g., *Korenaga and Karato*, 2008]; this assumes that the melt has been extracted. Assuming equilibrium fractionation of hydrogen upon melting leads to

$$\eta_F \propto \left[1 + F\left(D_H^{-1} - 1\right)\right]^p. \quad (1)$$

We limit the melt residue viscosity increase to 200 at most. The two parameterizations of melt residue viscosity are shown in Figure 1. We also consider several cases with a smaller melt residue viscosity increase.

3. Results

[20] The key feature of this study is the production of the crust from partial melting and the interaction of melt residue with mantle convection. We found that the partial melting is mainly controlled by two parameters: the mantle temperature and lithospheric thickness. The mantle temperature affects the rate of partial melting by changing the plume temperature. The mantle temperature can be modified either by changing the CMB temperature or by adjusting the internal heating rate in the mantle. Lithospheric thickness determines the minimal depth where the plume can ascend to cause the partial melting. We now present model calculations with different parameters.

[21] First, we ran a series of four cases where we considered two different values of the core-mantle boundary temperature T_{CMB} and both of the two parameterizations for the melt residue viscosity discussed above (see Table 2, cases 1–4 for parameters). The models were started from an initial temperature condition corresponding to a developed

Table 2. List of Cases

Case	T_{CMB} (K)	Q (W m^{-3})	η_F/Maximum	Steps	t_f (Myr)
1	2000	7.4×10^{-8}	continuous/200	80000	636
2	2100	7.4×10^{-8}	continuous/200	80000	694
3	2000	7.4×10^{-8}	step/200	81690	723
3b	2000	7.4×10^{-8}	step/100	80000	631
3c	2000	7.4×10^{-8}	step/50	54511	448
3d	2000	7.4×10^{-8}	step/1	54511	448
4	2100	7.4×10^{-8}	step/200	40354	352
5	2000	3.7×10^{-8}	step/200	95000	1131
6	2100	3.7×10^{-8}	step/200	80000	978
7	2200	3.7×10^{-8}	step/200	80888	880
K1	2200	7.4×10^{-8}		80000	685
K2	2200	3.7×10^{-8}		80000	1103
K3	2200	1.9×10^{-8}		80000	1335

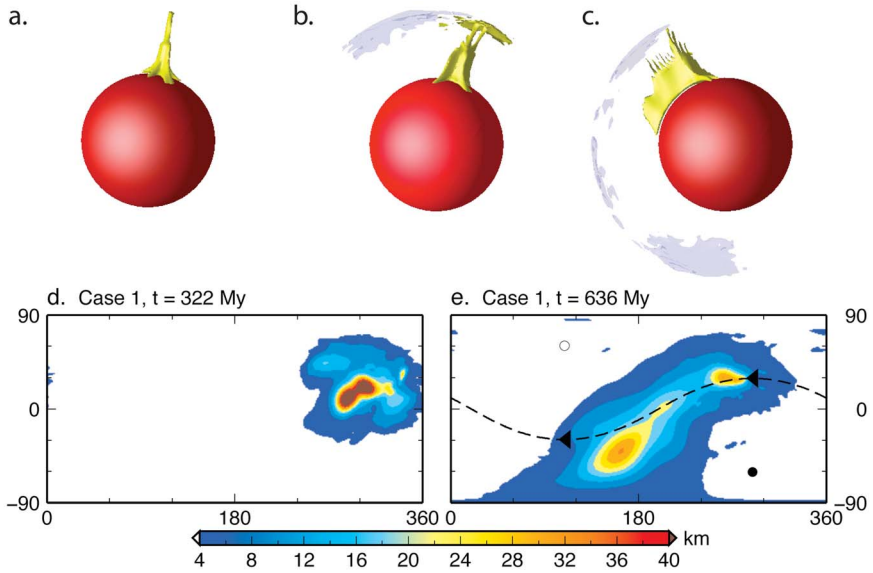

Figure 2. (a–c) Snapshots of temperature and degree of melting for case 1. An isosurface at +0.07 nondimensional temperature anomaly (130 K) is shown in yellow, and a 5% degree of melting contour is in blue. The thermal anomaly is not plotted in the upper 150 km. (d, e) Map view of crustal thickness. The color scale begins at 4 km and is saturated at 40 km. Figure 2a shows the initial condition, Figures 2b and 2d are at 322 Myr, and Figures 2c and 2e are at 636 Myr. The motion of the lithosphere is indicated with the rotation pole (black circle) and the great circle path (dashed line) of maximum surface velocity in Figure 2e.

spherical harmonic degree 1 flow (i.e., a single thermal upwelling) that is consistent with the model parameters [e.g., *Roberts and Zhong*, 2006]. The internal heating rate $Q = 7.4 \times 10^{-8}$ W m^{-3} corresponds to 90% of the heating rate at 4.56 Ga based on *Wanke and Dreibus*'s [1994] chemical abundances and results in a convecting mantle largely heated from within (by 80%–85% for cases 1–4).

[22] In Figure 2 we show the snapshots of temperature and melt residue and the map view of the crustal thickness for case 1 ($T_{CMB} = 2000$ K, continuous η_F). The initial one-plume temperature field is shown in Figure 2a; initially there is no crust and no melt residue. Figures 2b and 2d show the situation at 322 Myr after some melting occurred. A melt residue material has spread along the bottom of the lithosphere and forms an initial lithospheric root (seen as a 5% melt residue blue contour in Figure 2b). The new crustal production is relatively localized in a region above the upwelling (Figure 2d), but the lithosphere has already started to rotate relative to the plume, which can be seen from the ~30° angular separation between the plume and the keel center (Figure 2b). The melt generation and the plume- lithosphere relative rotation continue; by 636 Myr the initial melt residue keel has migrated by roughly 120° relative to the plume while new melt residue was added to the bottom of the lithosphere as the rotation proceeded (Figure 2c). The region of new thick crust is extended accordingly (Figure 2e).

[23] In Figure 3 we plot the amount of crustal material (Figure 3a) and average temperature (Figure 3b) against time for cases 1–4. The amount of crust is shown as the thickness of a global uniform layer of crustal material. We also show the amount of crust necessary to generate the dichotomy. Simply considering the difference between the two peaks in bimodal topography distribution of ~26 km [*Neumann*

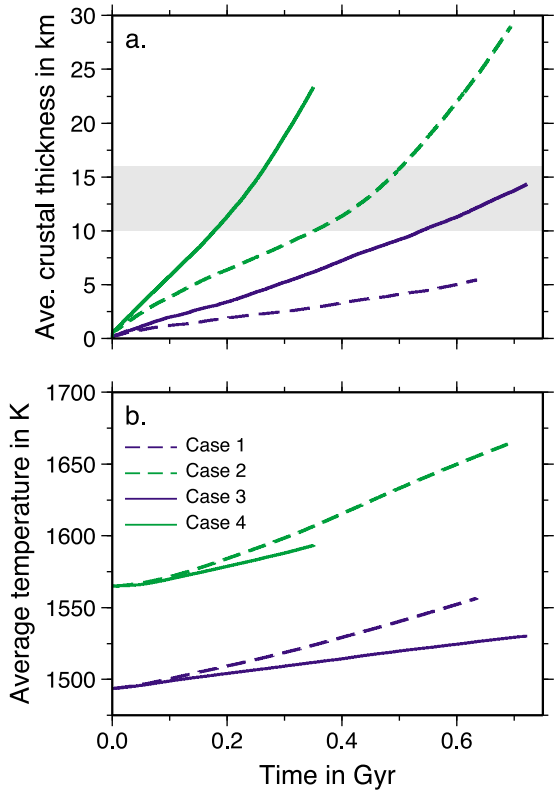

Figure 3. (a) Amount of crustal material and (b) the average temperature as functions of time for cases 1–4. Crustal volume is plotted as the thickness of an equivalent uniform global crustal layer. The amount of crust necessary to form the dichotomy is shown by gray shading.

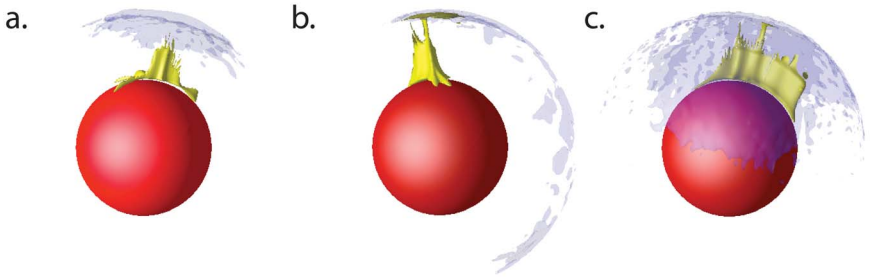

Figure 4. Snapshots of temperature and degree of melting for cases 2–4. See caption of Figure 2 for details. (a) Case 2 at 524 Myr, (b) case 3 at 710 Myr, and (c) case 4 at 348 Myr.

et al., 2004] and assigning half of the surface area to the highlands with thickened crust, we get a rough estimate of 13 km equivalent global crustal thickness required for the dichotomy formation. We highlight a region of 13 ± 3 km crustal thickness in Figure 3a.

[24] Snapshots of temperature and melt residue and the surface crustal thickness for cases 2–4 are shown in Figures 4 and 5, respectively. Case 2 differs from case 1 by an increased CMB temperature (T_{CMB} = 2100 K). The rate of melt generation is therefore higher than in case 1 (Figure 3a). Initially the crustal production is localized above the plume as in case 1, but because of mantle overheating (further discussed below) melting occurs globally after about 500 Myr (Figure 5a). Furthermore, as the mantle heats up the plume excess temperature becomes smaller and no relative rotation between the weaker upwelling and the lithosphere is observed (Figure 4a). Cases 3 and 4 are identical to cases 1 and 2, respectively, except that the step function melt residue viscosity parameterization was used (for these cases, the blue contour at 5% degree of melting in Figure 4 exactly traces the high-viscosity region). Their evolution (Figures 4b, 4c, 5b, and 5c) is qualitatively similar to cases 1 and 2, but they show differences in the amount of melt generation as well as the rate of mantle heating, as will be discussed in details later (Figure 3).

[25] The rate of melt production is sensitive to the dimensional CMB temperature. The value of the CMB temperature changes the dimensional mantle and plume temperature and their relation to the solidus. Increasing T_{CMB} from 2000 to 2100 K roughly triples the rate of melt production between otherwise identical models (i.e., compare cases 1 and 2 and cases 3 and 4).

[26] We also observe a strong effect of the melt residue on the thermal evolution, and its sensitivity to the chosen melt residue viscosity dependence on the degree of melting. Initially the melting region within the hot plume spans a depth range of ~50–200 km. The stiff melt residue material sticks to the bottom of the thermal lithosphere and increases the local lithospheric thickness. This effective thickening of the thermal boundary layer results in decrease in the conductive heat transport to the surface. As a result the mantle temperature and consequently the plume temperature increases (Figure 3b) and this moves the base of the melting zone to larger depths (up to 400 km depth), thus enhancing the melting.

[27] In cases with continuously varying melt residue viscosity, the effect of the stiff melt residues is more pronounced relative to cases with a step function melt residue viscosity. With the step function η_F, the melt residue stiffening does not come into play until the degree of melting reaches the chosen threshold of 5%. With continuous η_F, the viscosity of the melt residue increases significantly for relatively small values of degree of melting; for example, the viscosity increases by a factor of 10 at F = 2.2% (Figure 1). The melt residue hinders the flow and thickens the thermal boundary layer starting at low values of degree of melting. As a result, the melt production is inhibited while the temperature increases more rapidly in cases with continuous η_F relative to cases with a step function η_F (Figure 3).

[28] In cases 1–4 discussed above we set the maximum melt residue viscosity increase to 200. In order to investigate whether this choice has any significant effect on the outcome we computed two additional cases, 3b and 3c, which are identical to case 3 except for the melt residue viscosity

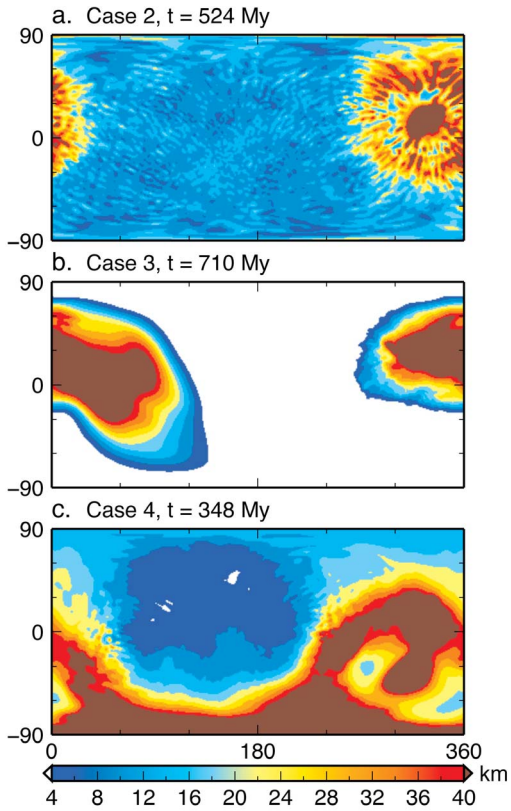

Figure 5. Map view of crustal thickness at the surface for cases 2–4. The color scale begins at 4 km and is saturated at 40 km (same as in Figure 2).

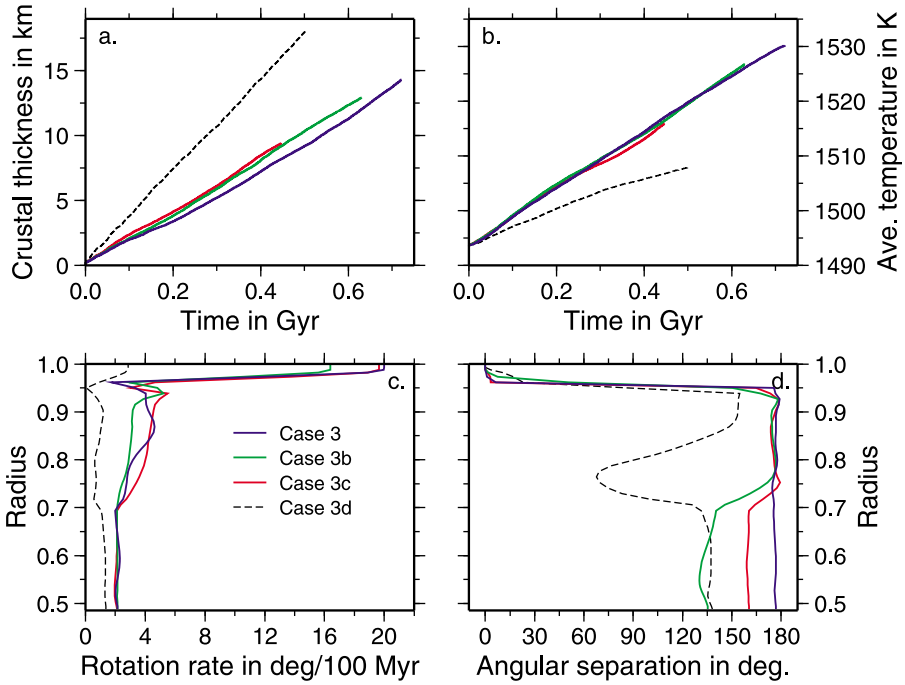

Figure 6. Comparison of cases 3–3d, which differ in the melt residue viscosity value. (a) Amount of crustal material and (b) the average temperature as functions of time; (c) rotation rate and (d) angular distance of rotation pole from the reference rotation pole of the surface as functions of nondimensional radius at 350 Myr.

contrast which was lowered to 100 and 50, respectively. We also include case 3 d where the residue lacks any viscosity contrast (i.e., η_F = 1; Table 2). In Figure 6 we show the comparison of the crustal production (Figure 6a) and mantle temperature (Figure 6b) over time. Cases 3, 3b, and 3c give essentially identical results, while case 3 d shows faster crustal production and slower mantle temperature increase because of the absence of the stiff melt residue effects. The convection calculations were performed in a reference frame with no net rotation of the entire mantle [*Zhong et al.*, 2008]. Individual spherical horizontal layers can, however, exhibit a nonzero rotation in this reference frame, if lateral variations in viscosity exist in the mantle [e.g., *Zhong*, 2009]. For each layer of finite elements, we can find the coordinates of the rotation pole and the angular rotation rate. In Figure 6 we show the rotation rates (Figure 6c) and the relative position of the rotation poles with respect to the surface layer pole (Figure 6d) for cases 3 through 3 d at time of 350 Myr. The relative rotation between the lithosphere and the mantle is clearly seen in Figures 6c and 6d, and the amplitude of the rotation of ∼20°/100 Myr is very similar between cases 3, 3b, and 3c. We therefore conclude that the lithosphere-mantle rotational dynamics are insensitive to the exact value of the melt residue viscosity increase in the explored range of 50 to 200. The lack of significant rotation in case 3 d clearly demonstrates that melt residue stiffening is necessary for the proposed mechanism. Temperature-dependent viscosity alone, although causing lateral variations in mantle viscosity, is not efficient in causing the rotation as was already shown by *Zhong* [2009] and *Šrámek and Zhong* [2010].

[29] The strong coupling between melt generation, and the thermal evolution and mantle flow that we observe in the models is expected when the stiffening of the melt residue is considered. If we let the cases just presented evolve further in time, the temperature would continue to increase, resulting in further melting and more melt residue, which would then feed back and further increase the temperature because of insulation by the thickening lithosphere. In the present model, the internal heating rate as well as the CMB temperature are kept constant in time. In a real planet, however, the internal radiogenic heat sources would decay with time and the core would cool down as it loses heat to the mantle. Furthermore, fractionation of heat producing elements into the crust (not modeled here) would modify the internal heat source distribution in the mantle. In this modeling, we choose not to account for all these additional effects, but rather employ a simple modification in the following cases.

[30] In cases 5–7 (Table 2) we reduced the internal heating rate to one half of the chondritic heating rate at 4.5 Ga. As a simple rationale, this may reflect a previous fractionation of heat producing elements into a primordial crust of uniform thickness, not contributing to the dichotomy. The models are started from the same initial temperature condition as cases 1–4 which now represents a warmer mantle than what corresponds to the model parameters, and therefore the mantle may cool down with time. The ratio of internal to bottom heating decreases with time in cases 5–7 but internal heating remains dominant (bottom heating accounts for 30% of the surface heat loss at most). Cases 5–7 differ in the CMB temperature; it was set to 2000, 2100, and 2200 K in cases 5, 6, and 7, respectively (Table 2). Rather

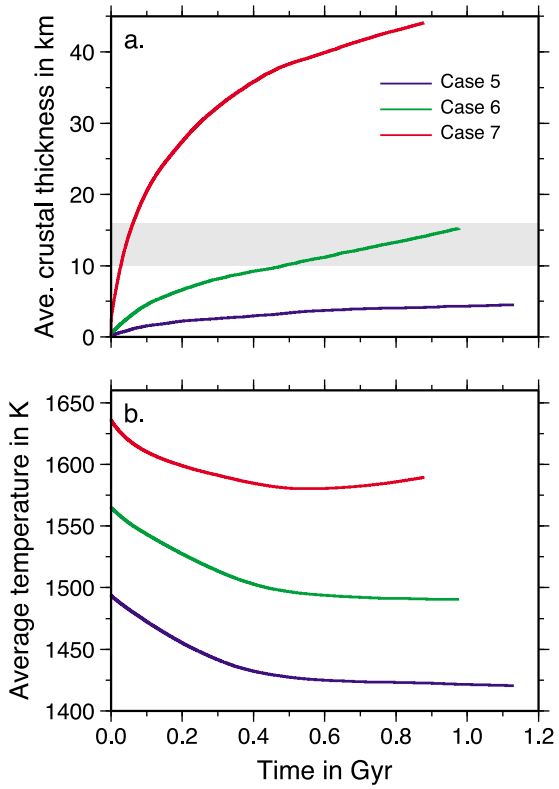

Figure 7. (a) Amount of crustal material and (b) the average temperature as functions of time for cases 5–7. Crustal volume is plotted as the thickness of an equivalent uniform global layer. The amount of crust necessary to form the dichotomy is shown by gray shading.

than computing cases with both parameterizations of the melt residue viscosity dependence as we did in cases 1–4, in the following we only use the step function melt residue viscosity. Of course, both parameterizations are only simplifications of the actual dehydration stiffening and may be considered the end-member cases of the real behavior. The relative trends between the two descriptions were seen in cases 1–4; in cases 5–7 the continuously varying melt residue viscosity would result in somewhat slower mantle cooling and smaller crustal thickness than the step function melt residue viscosity. From a numerical perspective, a step viscosity increase for the melt residue viscosity gives better convergence of the numerical solutions and faster run time.

[31] Cases 5–7 were run for a duration of 900–1000 Myr. The temporal evolution of the crustal production and the average temperature is shown in Figure 7. The average mantle temperature now decreases with time, as the reduced internal heating more than compensates for the insulating effect of the stiff melt residue. Only in the case with the hottest CMB (2200 K, case 7) the mantle temperature starts to increase again toward the end of the calculation; this is caused by the insulating effect of a thick, essentially global melt residue layer that forms in this case.

[32] In addition to the time evolution of the total crustal volume shown in Figure 7a, we show the map view of the crustal thickness in Figure 8. As expected and already observed in previous cases, the amount of melting depends strongly on the mantle temperature. For low T_{CMB} (2000 K, case 5), the melt production is restricted to a small region above the upwelling; in Figure 8a we show the crustal thickness at the end of the calculation run. The volume of new crust is relatively small and insufficient to explain the dichotomy (Figure 7a).

[33] For high T_{CMB} (2200 K, case 7), a large volume of melt is quickly produced which exceeds the melt volume needed to form the dichotomy (Figures 8b and 7a). Even though the thickest crust is produced above the plume,

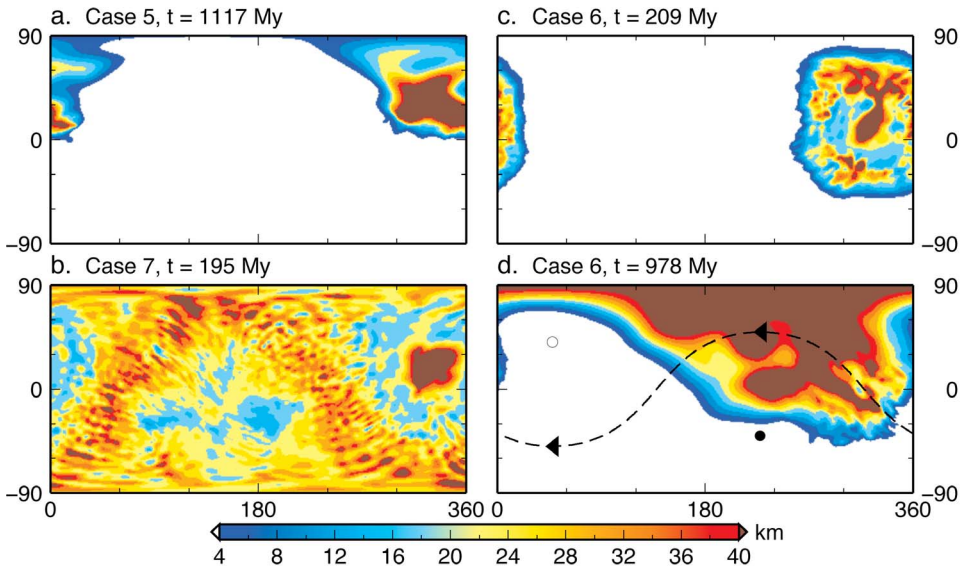

Figure 8. Map view of crustal thickness. The color scale begins at 4 km and is saturated at 40 km (as in Figures 2 and 5). The motion of the lithosphere is indicated with the rotation pole (black circle) and the great circle path (dashed line) of maximum surface velocity in Figure 8d.

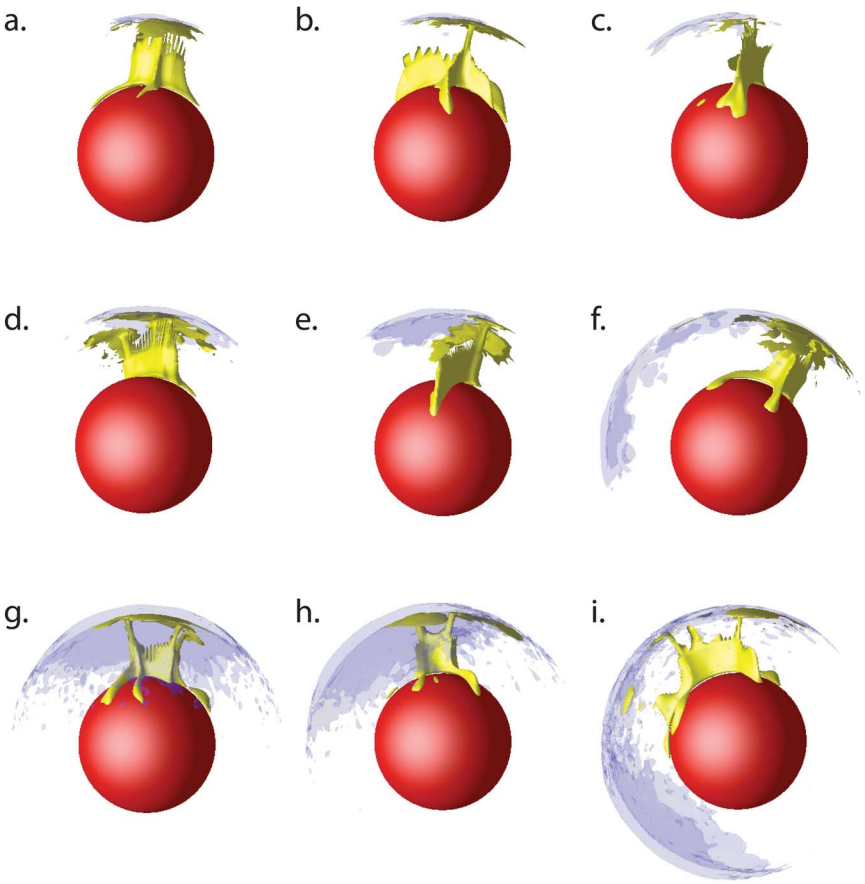

Figure 9. Snapshots of temperature and degree of melting for cases 5–7. An isosurface at +0.07 nondimensional temperature anomaly (130 K) is shown in yellow, and a 5% degree of melting contour is in blue. The thermal anomaly is not plotted in the upper 150 km. Case 5 at (a) 185 Myr, (b) 393 Myr, and (c) 908 Myr; case 6 at (d) 209 Myr, (e) 458 Myr, and (f) 978 Myr; case 7 at (g) 195 Myr, (h) 387 Myr, and (i) 625 Myr.

significant melt production occurs globally, including the hemisphere antipodal to the plume. Here, the thickness of the crust appears to be elevated along a circular path around the plume centers (Figure 8b). This is caused by the modulation of the large-scale flow by the stiff melt residue. The initial extensive melting within the upwelling produces a sizable melt residue region. This later prevents the convecting mantle to reach the melting depth at this location. The flow is diverted and most melting then occurs around the edges of the early melt residue domain where the melting depth can be reached. We stress that this is not a manifestation of lateral melt transport (not modeled here) but merely reflects a horizontal variability in the melt production due to lithospheric thickness variations; this is an observation relatively early in the evolution (at 195 Myr, corresponding to the snapshot in Figure 9g) before any significant rotation of the lithosphere occurs.

[34] At intermediate T_{CMB} (2100 K, case 6), the volume of generated melt is comparable to the amount required to form the dichotomy (Figure 7a). Initially, melting is relatively localized (Figure 8c). Later when the upwelling begins to migrate relative to the lithosphere, the region of significant crustal thickness broadens and eventually reaches a roughly hemispheric extent (Figure 8d).

[35] Relative motion between the lithosphere and the upwelling of various amplitudes is observed in most cases discussed here; we will focus the discussion on cases 5–7. In Figure 10 we show the rotation rates (Figure 10, left) and the relative position of the rotation poles with respect to the surface layer pole (Figure 10, right) for cases 5–7 at several different times. In case 5 the amount of melting is quite small, and therefore the volume of the high-viscosity melt residue (above 5% melting) is relatively insignificant, laterally spanning a region of just few tens of degrees in angular extent (see snapshots in Figures 9a–9c). Some rotation of the lithosphere relative to the upwelling can be seen but the rotation rate is small (Figure 10a) and a relative rotation of only about 20° is reached (Figure 9c). Moreover, there seems to be some decoupling between the average rotation of the low-viscosity upper mantle and higher-viscosity lower mantle (Figure 10b).

[36] Cases 6 and 7 show a consistent rotation between the lithosphere and the underlying mantle; here the net rotation of the upper mantle is identical to that of the lower mantle (Figures 10c–10f). As the upwelling moves away from below the thickest melt residue, more melt and residue are being generated, which broadens the region with significant crustal thickness and drives further rotation. A total amount

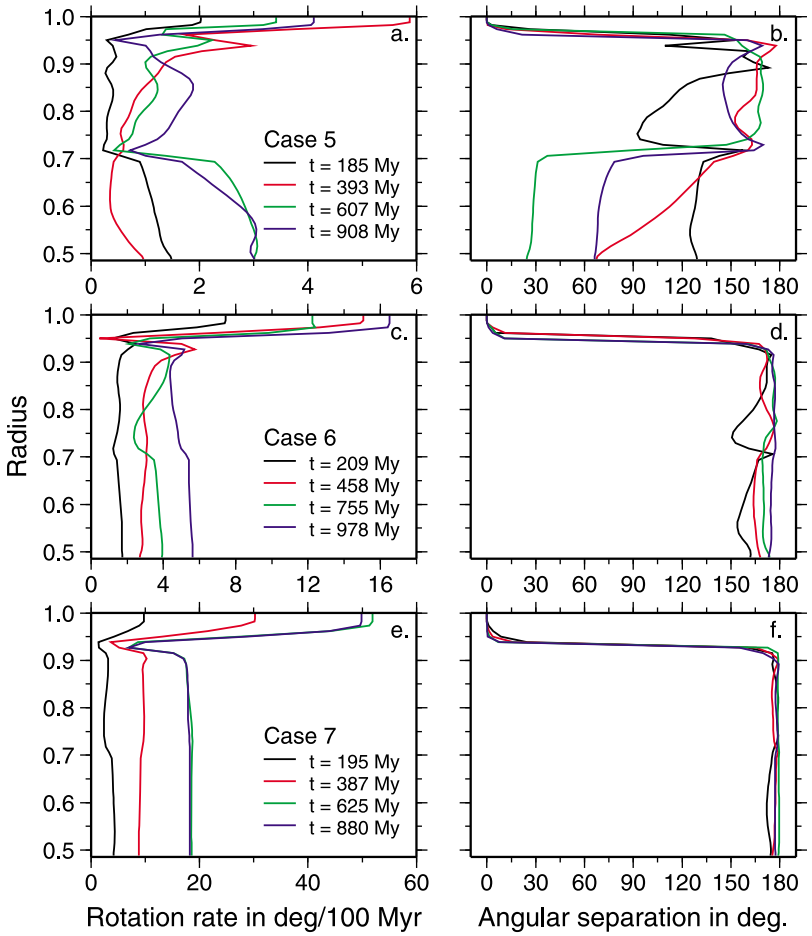

Figure 10. (left) Rotation rate and (right) angular distance of rotation pole from the reference rotation pole of the surface as functions of nondimensional radius for cases (a, b) 5, (c, d) 6, and (e, f) 7.

of lithospheric relative rotation with respect to the plume of over 120° was reached(Figures 9f and 9i). Maximum angular separation rates between the lithosphere and the upwelling of ∼20°/100 Myr in case 6 and ∼70°/100 Myr in case 7 were observed.

4. Cessation of Plume Migration

[37] In the framework of this model, an important question is what causes the volcanic center to stabilize near the dichotomy boundary or Tharsis for the last ∼3.5 Gyr. In our previous studies [*Zhong*, 2009; *Šrámek and Zhong*, 2010] where the lithospheric keel was imposed rather than generated by melting, the relative motion between the lithosphere and the upwelling ceased when the upwelling reached the edge of the keel. Of course, secular cooling of Mars should decrease the rate of melt production, and therefore the melt residue generation will slow down, resulting in a smaller lithospheric thickness variation. A particularly high rate of secular cooling has been suggested during Noachian, as evidenced from the abrupt increase of the inferred elastic thickness of the lithosphere for ages prior to the end of Noachian [*McGovern et al.*, 2002]. This rapid cooling was possibly caused by efficient hydrothermal heat transfer in the fractured, water saturated layer of the upper crust which may have reached down to depth of ∼10 km [*Parmentier and Zuber*, 2007]. The secular cooling would slow down the migration of the plume relative to the lithosphere but may not be sufficient to essentially shutdown the relative rotation completely. Another effect of cooling of the planet is the increase of the interior viscosity, including the upper mantle viscosity. The more sluggish flow, particularly in the upper mantle below the lithosphere, should also contribute to the shutoff of the plume migration.

[38] We devised a way to investigate the effect of mantle viscosity on the magnitude of the plume-lithosphere relative rotation rate. The goal is to compare the rotation rates for cases that differ in mantle viscosity but are otherwise identical; most importantly cases with identical lithospheric thickness variation. Therefore we considered cases K1–K3 (Table 2) without partial melting where a lithospheric keel of a hemispheric extent is imposed at the outset, rather than generated from convection and partial melting. The geometry we used for the keel is identical to keel A of *Šrámek and Zhong* [2010]; it is 260 km thick at the center and its thickness decreases linearly with angular distance from the center down to zero at 90° arc distance from the keel center. The three cases are started from identical initial thermal condition (the same as in cases 1–7) and the keel is initially centered above the plume. The only difference between the cases K1–K3 is the value of the internal heating rate that determines the cooling rate of the mantle (Table 2).

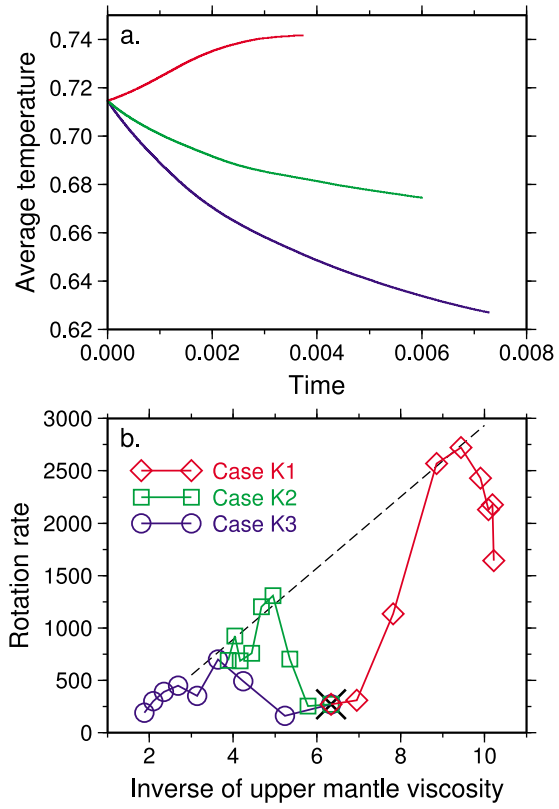

Figure 11. (a) Average nondimensional temperature as a function of nondimensional time and (b) nondimensional rotation rate versus the inverse of nondimensional upper mantle viscosity for cases K1–K3. A linear fit to the maximum value in each case is shown as a black dashed line.

[39] In Figure 11, we show the average temperature as a function of time and the lithosphere-mantle relative rotation rate as a function of upper mantle viscosity for cases K1–K3. The difference in internal heating rate results in different evolution of the mantle temperature (Figure 11a) and therefore of the value of temperature-dependent viscosity in the upper mantle (Figure 11b) between these cases. The common initial state is indicated by a black cross in Figure 11b. In all the three cases, we can identify an initial stage when the relative rotation rate between the lithosphere and the mantle increases. Then the rotation rate reaches a maximum value which corresponds to the fastest migration of the plume away from the center of the keel. Later, when the plume approaches the keel edge, the rotation slows down again. Despite the temporal variability of the rotation rate within each case, there is a clear trend for a characteristic relative rotation rate to decrease with increasing viscosity. It appears that the maximum relative rotation rate is proportional to the inverse of upper mantle viscosity (showed as dashed line in Figure 11b).

[40] Overall, it seems that the development of the lithospheric keel edge (i.e., the dichotomy boundary) and the stabilization of the plume (i.e., Tharsis) center near it in the last ~3.5 Gyr could be explained as the effect of secular cooling, through a combination of diminishing rate of melt production, increasing of upper mantle viscosity, and remelting of previously devolatilized material at later times leading to negligible viscosity increase of the melt residue. Subsequent plume melting would not substantially modify the keel edge, and we have already shown in a previous study that the upwelling can remain essentially stationary relative to the keel edge [*Šrámek and Zhong*, 2010].

5. Discussion

[41] In this work we newly test an important aspect of the "rotation of the lithosphere" model for Mars of *Zhong* [2009]. Our previous modeling efforts [*Zhong*, 2009; *Šrámek and Zhong*, 2010] assumed that the process of hemispheric dichotomy formation left behind a deep lithospheric keel below the thicker highland crust, and examined how such a lithospheric keel excited relative rotation of lithosphere with respect to the underlying mantle and mantle plume, thus offering a possible mechanism to unify the formation of crustal dichotomy and Tharsis. Here we investigated whether such a lithospheric keel can be generated self-consistently as a devolatilized residue material after partial melting, and whether such dynamically generated lithospheric keels and thickness variations can produce lithospheric rotation relative to the mantle.

[42] There are some general points to be made. Rather obviously, the amount of partial melting strongly depends on the dimensional mantle temperature; in this study we used partial melting parameterization by *Katz et al.* [2003] but this finding is general. For example, increasing the CMB temperature from 2000 to 2200 K between our models 5 to 7 causes the melting rate to increase by a factor of roughly 10. Of course, a low enough mantle temperature would produce no melting while further increasing the temperature would eventually lead to catastrophic melting in a laterally continuous layer. The amount of melting is further complicated by water content of the mantle that may affect the melting temperature significantly [e.g., *Médard and Grove*, 2006]. Here, we only want to emphasize that given some proper mantle conditions (e.g., CMB temperature, mantle internal heating rates and water content), mantle melting from one-plume convection may generate additional crust that is adequate to account for the crustal dichotomy.

[43] Accounting for the viscosity increase of a devolatilized melt residue [*Pollack*, 1986; *Hirth and Kohlstedt*, 1996] introduces a strong coupling between the partial melting, the convective flow in the mantle and the thermal evolution. A melt residue layer generated by an early melting may add to the local lithospheric thickness, prevent the upwelling to reach melting depth, deflect the flow laterally and change the location of subsequent melting. A large lithospheric thickness variation then results in a rotation of the one-plate lithosphere relative to the mantle below. Of course, the degree of melting–melt residue viscosity dependence for the melt residue is likely more complicated than the simple parameterizations that we used here. It may even vary regionally, especially if isolated pockets of melt remain trapped at melting depths in some areas, in which case the melt residue may in fact be locally weakened. Here we wanted to keep the model relatively simple and did not consider these complexities.

[44] The melt generated at depth and extracted to the surface is interpreted as the crustal material of Mars. It represents the additional thick crust in the highlands. Case 6

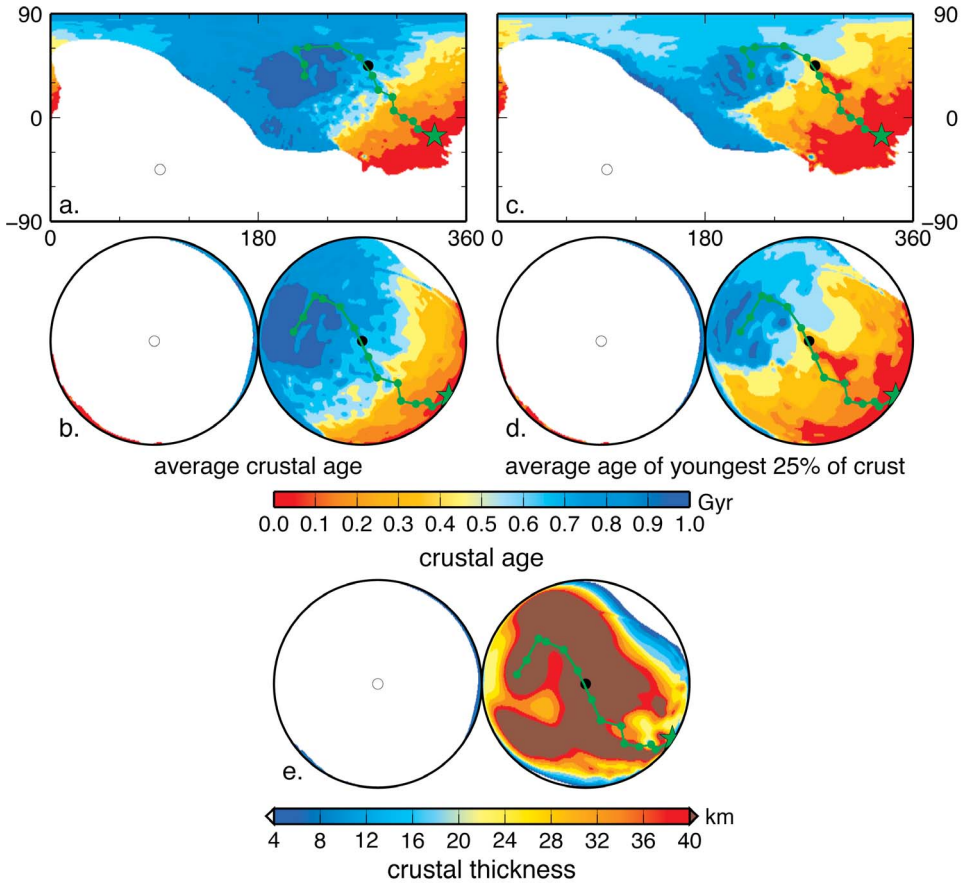

Figure 12. Maps of (a, b) average crustal age, (c, d) average age of the youngest 25% of the crust, and (e) crustal thickness for case 6 at 978 Myr (as in Figure 8d). Crustal ages are not shown in areas where the thickness of crust generated by convection is below 4 km. The centers of the orthographic hemispherical projections in Figures 12b, 12d, and 12e are indicated by circles in Figures 12a and 12c. The current center of the thermal upwelling (calculated at midmantle depth) is indicated by a green star, and its past track is shown as a green line.

broadly satisfies the observational constraints on the crustal volume and its spatial distribution, necessary to generate the dichotomy. This thick highland crust is generated continuously, over a period of several hundred million years, above the one thermal upwelling in the mantle. As the one-plate lithosphere develops the thickness variation due to the presence of the high-viscosity melt residue, it migrates relative to the upwelling at a rate of 10°–20°/100 Myr. As melting continues, the crustal material ends up distributed over an extensive region, rather than being piled up locally in a narrow zone. The hemispheric extent of the thick crust regions can be seen in Figure 12, where we plot the crustal thickness for case 6 at time 978 Myr in orthographic hemispherical projection (Figure 12e). We also show a map of the average crustal age (Figures 12a and 12b) and the average age of the youngest 25% of the crust (Figures 12c and 12d). The location of the thermal upwelling center and its past migration relative to the lithosphere are also shown in Figure 12. There is a clear progression of crustal ages from the oldest ages near one side of the thick crust region where the upwelling was originally located toward the other edge to which the plume migrated. The older terrains would correspond to the eastern side of the southern highlands while the younger crust would represent the western (Tharsis) region, even though the crustal age variation in this model shows larger amplitude that what is generally accepted for the southern highlands of Mars. We propose that the crustal dichotomy may have been generated by this mechanism. It may be extremely difficult to find clear geologic evidence of the proposed scenario, given the ancient age of the features. However, the new analysis of *Hynek et al.* [2011] based on geologic mapping, crater morphometry and age dating, and examination of crustal magnetic signature provides some observational evidence for this model. *Hynek et al.* [2011] argue for a plume track from near the center of the dichotomy toward Tharsis region manifested as extensive volcanic resurfacing of older cratered terrains. The present modeling results do not provide a clear match to their observation, even though Figure 12d hints at some late crustal addition along the plume track.

[45] Our model of relative motion between the lithospheric shell and the underlying mantle and mantle plume may have implications for true polar wander (TPW), even though they are caused by different physical mechanisms, as already pointed out by *Zhong* [2009]. The rotation of the lithosphere may generate similar tectonic features to those

expected for TPW (such as stress patterns related to the deformation of rotational bulge), in particular in the case where the axis of relative rotation between lithosphere and the mantle differs significantly from the spin axis [*Zhong*, 2009]. TPW on Mars has been a controversial topic. Significant TPW (>50°) in the last 4 Gyr was suggested in studies on paleomagnetic poles [*Arkani-Hamed and Boutin*, 2004; *Hood et al.*, 2005] and deformed ancient shorelines [*Perron et al.*, 2007] while TPW during or prior to Early Noachian (4.08–3.93 Ga) was inferred from the analysis of the moment of inertia from the Martian crustal dichotomy [*Roberts and Zhong*, 2007]. However, the lack of global tectonic deformation predicted from TPW calculations [*Melosh*, 1980; *Grimm and Solomon*, 1986] and stabilizing effect of thick elastic shell on the spin axis [*Willemann*, 1984] were used as evidence for negligible TPW on Mars, although recent theoretical work by *Matsuyama et al.* [2006] indicated that significant post-Tharsis TPW is possible, which provided the basis to interpret the paleoshorelines in terms of TPW [*Perron et al.*, 2007]; recently, *Matsuyama and Manga* [2010] have reduced somewhat estimates of likely TPW. Our proposed relative motion of lithosphere shell and the mantle plume is concurrent with formation of the crustal dichotomy and predates Tharsis, and it is possible that the variations in paleomagnetic pole locations [*Arkani-Hamed and Boutin*, 2004; *Hood et al.*, 2005] may result from our proposed scenario rather than TPW. It remains to be assessed how TPW and our proposed motion of lithosphere shell relative to the underlying mantle may manifest themselves in surface deformation.

[46] The present model contains several simplifying assumptions that need to be discussed. First, an obvious objection to the present model is the use of the initial condition with a fully developed spherical harmonic degree 1 flow (i.e., a single upwelling), although such a degree 1 flow develops dynamically self-consistently for the given viscosity structure [e.g., *Roberts and Zhong*, 2006]. Some melting must have occurred prior to our starting point during the earliest Martian evolution that led to a long-wavelength flow. This early melting generated some primordial crust, arguably more uniformly distributed over the surface. This early crustal production may have generated a relatively uniform global crust (that is, a nonzero crustal thickness inferred for the thinner crust of the northern hemisphere), together with magma ocean solidification process [e.g., *Elkins-Tanton et al.*, 2003]. An early melting episode would have extracted some water from the mantle. The issue of early devolatilization is still debated. While *Fraeman and Korenaga* [2010] argue for an efficient early loss of initial mantle water content, other studies suggest much more limited or more gradual mantle dehydration [e.g., *Hauck and Phillips*, 2002; *Grott et al.*, 2011]. It is therefore possible that significant amount of water remained in the mantle after an early crustal production that preceded the sequence proposed in our model. In this study we wanted to investigate the important aspect of global melt generation in degree 1 convection and the dynamical coupling between the stiff melt residue and the convecting mantle. A more complete model of Martian evolution would involve additional complexities, in particular the question of the postaccretion state of the Martian mantle and the appropriate initial condition, which becomes more important when melting is included in the model. The dynamic effect of the viscous melt residue does introduce an additional strong coupling between the thermal evolution and the melting; it will be interesting to explore to what extent this feedback might affect the development of the preferred convective planform. In particular, future efforts need to address whether such more complete model that links the immediate postaccretion/postdifferentiation state to subsequent thermal evolution can satisfy all the constraints on the inferred time sequence of dichotomy and Tharsis formation.

[47] Second, fractionation of heat-producing elements into the crust is not modeled. This effect would feed back to the long-term thermal evolution of the mantle and limit the crustal production at later times. We can estimate the degree of fractionation using a simple calculation. For example, at the end of computation of case 6 a mass fraction of 34% of the mantle experienced at least 1% melting. Assuming that the crust was generated by melting of 34% of the mantle, the average degree of melting is ∼4%. For the highly incompatible heat producing elements (HPE; i.e., U, Th, K) this translates into 25-fold enrichment in HPE of the crust relative to the initial mantle composition and depletion of the residual mantle by 1/3 on average. Moreover, we keep the internal heating rate constant with time, rather than have it decay exponentially. This also overestimates the mantle temperatures at later stages.

[48] Third, we assume for simplicity that all the melt is instantaneously extracted to the surface. The complexities of melt extraction, such as extrusion at surface versus subsurface intrusion in the crust, or possible trapping of melt at large depth or refreezing, are not considered (for an example of a coupled magma-mantle dynamics model, see, e.g., *Katz* [2010]). Nor does the model include lateral transport of melt at or below the surface; such crustal flow may result in modification of the crustal thickness distribution. In fact, as pointed out by *Zhong* [2011], properly accounting for the crustal flow during and immediately after the dichotomy formation and comparing it against the present-day inferred crustal thickness [*Neumann et al.*, 2004] will be a necessary step to validate any model for the dichotomy formation, endogenic or exogenic, and possibly discriminate between different hypotheses.

[49] Considering the aforementioned effects would modify, to various degrees, the modeled melt production curves and crustal distribution patterns, but would not change our main conclusions.

6. Conclusions

[50] We have formulated 3-D spherical shell convection models for Martian mantle where we included partial melting and the effect of melt residue stiffening. The amount of melting is highly sensitive to the mantle temperature and further coupling between melting, mantle flow and thermal evolution is introduced through the high-viscosity melt residue. We show that lithospheric thickness variation and a corresponding crustal thickness variation with a hemispheric extent can be generated by partial melting in the Martian mantle with a spherical harmonic degree 1 convection pattern (i.e., single thermal upwelling). Rotation of a one-plate lithosphere with respect to the upwelling and the underlying mantle can then be excited. This may offer an endogenic

mechanism for the generation of the Martian crustal dichotomy and subsequent evolution of the Tharsis volcanic province.

[51] **Acknowledgments.** This work was supported by NASA MFRP grant award NNX08AN12G. We wish to thank the Associate Editor and an anonymous reviewer for their thoughtful reviews.

References

Anderson, R. C., J. M. Dohm, M. P. Golombek, A. F. C. Haldemann, B. J. Franklin, K. L. Tanaka, J. Lias, and B. Peer (2001), Primary centers and secondary concentrations of tectonic activity through time in the western hemisphere of Mars, *J. Geophys. Res.*, *106*(E9), 20,563–20,585, doi:10.1029/2000JE001278.

Andrews-Hanna, J. C., M. T. Zuber, and W. B. Banerdt (2008), The Borealis basin and the origin of the Martian crustal dichotomy, *Nature*, *453*(7199), 1212–1215, doi:10.1038/nature07011.

Arkani-Hamed, J., and D. Boutin (2004), Paleomagnetic poles of Mars: Revisited, *J. Geophys. Res.*, *109*, E03011, doi:10.1029/2003JE002229.

Banerdt, W. B., M. P. Golombek, and K. L. Tanaka (1992), Stress and tectonics on Mars, in *Mars*, edited by H. H. Kieffer et al., chap. 8, pp. 249–297, Univ. of Ariz. Press, Tucson.

Bertka, C. M., and J. R. Holloway (1994), Anhydrous partial melting of an iron-rich mantle I: Subsolidus phase assemblages and partial melting phase relations at 10 to 30 kbar, *Contrib. Mineral. Petrol.*, *115*(3), 313–322, doi:10.1007/BF00310770.

Breuer, D., H. Zhou, D. A. Yuen, and T. Spohn (1996), Phase transitions in the Martian mantle: Implications for the planet's volcanic history, *J. Geophys. Res.*, *101*(E3), 7531–7542, doi:10.1029/96JE00117.

Carr, M. H., and H. Wänke (1992), Earth and Mars: Water inventories as clues to accretional histories, *Icarus*, *98*(1), 61–71, doi:10.1016/0019-1035(92)90207-N.

Elkins-Tanton, L. T., E. M. Parmentier, and P. C. Hess (2003), Magma ocean fractional crystallization and cumulate overturn in terrestrial planets: Implications for Mars, *Meteorit. Planet. Sci.*, *38*(12), 1753–1771, doi:10.1111/j.1945-5100.2003.tb00013.x.

Elkins-Tanton, L. T., P. C. Hess, and E. M. Parmentier (2005), Possible formation of ancient crust in Mars through magma ocean processes, *J. Geophys. Res.*, *110*, E12S01, doi:10.1029/2005JE002480.

Fraeman, A. A., and J. Korenaga (2010), The influence of mantle melting on the evolution of Mars, *Icarus*, *210*(1), 43–57, doi:10.1016/j.icarus.2010.06.030.

Frey, H. (1979), Thaumasia: A fossilized early forming Tharsis uplift, *J. Geophys. Res.*, *84*(B3), 1009–1023, doi:10.1029/JB084iB03p01009.

Frey, H., and R. A. Schultz (1988), Large impact basins and the mega-impact origin for the crustal dichotomy on Mars, *Geophys. Res. Lett.*, *15*(3), 229–232, doi:10.1029/GL015i003p00229.

Grimm, R. E., and S. C. Solomon (1986), Tectonic tests of proposed polar wander paths for Mars and the Moon, *Icarus*, *65*(1), 110–121, doi:10.1016/0019-1035(86)90066-7.

Grott, M., A. Morschhauser, D. Breuer, and E. Hauber (2011), Volcanic outgassing of CO_2 and H_2O on Mars, *Earth Planet. Sci. Lett.*, *308*(3–4), 391–400, doi:10.1016/j.epsl.2011.06.014.

Harder, H., and U. R. Christensen (1996), A one-plume model of Martian mantle convection, *Nature*, *380*(6574), 507–509, doi:10.1038/380507a0.

Hartmann, W. K. (1973), Martian surface and crust: Review and synthesis, *Icarus*, *19*(4), 550–575, doi:10.1016/0019-1035(73)90083-3.

Hauck, S. A., II, and R. J. Phillips (2002), Thermal and crustal evolution of Mars, *J. Geophys. Res.*, *107*(E7), 5052, doi:10.1029/2001JE001801.

Herzberg, C., P. Raterron, and J. Zhang (2000), New experimental observations on the anhydrous solidus for peridotite KLB-1, *Geochem. Geophys. Geosyst.*, *1*(11), 1051, doi:10.1029/2000GC000089.

Hirth, G., and D. L. Kohlstedt (1996), Water in the oceanic upper mantle: Implications for rheology, melt extraction and the evolution of the lithosphere, *Earth Planet. Sci. Lett.*, *144*(1–2), 93–108, doi:10.1016/0012-821X(96)00154-9.

Hood, L. L., C. N. Young, N. C. Richmond, and K. P. Harrison (2005), Modeling of major Martian magnetic anomalies: Further evidence for polar reorientations during the Noachian, *Icarus*, *177*(1), 144–173, doi:10.1016/j.icarus.2005.02.008.

Hynek, B. M., S. J. Robbins, O. Šrámek, and S. J. Zhong (2011), Geological evidence for a migrating Tharsis plume on early Mars, *Earth Planet. Sci. Lett.*, *310*(3–4), 327–333, doi:10.1016/j.epsl.2011.08.020.

Johnson, C. L., and R. J. Phillips (2005), Evolution of the Tharsis region of Mars: Insights from magnetic field observations, *Earth Planet. Sci. Lett.*, *230*(3–4), 241–254, doi:10.1016/j.epsl.2004.10.038.

Katz, R. F. (2010), Porosity-driven convection and asymmetry beneath mid-ocean ridges, *Geochem. Geophys. Geosyst.*, *11*, Q0AC07, doi:10.1029/2010GC003282.

Katz, R. F., M. Spiegelman, and C. H. Langmuir (2003), A new parameterization of hydrous mantle melting, *Geochem. Geophys. Geosyst.*, *4*(9), 1073, doi:10.1029/2002GC000433.

Ke, Y., and V. S. Solomatov (2006), Early transient superplumes and the origin of the Martian crustal dichotomy, *J. Geophys. Res.*, *111*, E10001, doi:10.1029/2005JE002631.

Keller, T., and P. J. Tackley (2009), Towards self-consistent modeling of the Martian dichotomy: The influence of one-ridge convection on crustal thickness distribution, *Icarus*, *202*(2), 429–443, doi:10.1016/j.icarus.2009.03.029.

Kiefer, W. S. (2003), Melting in the Martian mantle: Shergottite formation and implications for present-day mantle convection on Mars, *Meteorit. Planet. Sci.*, *38*(12), 1815–1832, doi:10.1111/j.1945-5100.2003.tb00017.x.

King, S. D., and H. L. Redmond (2005), The crustal dichotomy and edge driven convection: A mechanism for Tharsis Rise volcanism?, *Lunar Planet. Sci.*, *XXXVI*, Abstract 1960.

Korenaga, J., and S. Karato (2008), A new analysis of experimental data on olivine rheology, *J. Geophys. Res.*, *113*, B02403, doi:10.1029/2007JB005100.

Kushiro, I., Y. Syono, and S. Akimoto (1968), Melting of a peridotite nodule at high pressures and high water pressures, *J. Geophys. Res.*, *73*(18), 6023–6029, doi:10.1029/JB073i018p06023.

Lenardic, A., F. Nimmo, and L. Moresi (2004), Growth of the hemispheric dichotomy and the cessation of plate tectonics on Mars, *J. Geophys. Res.*, *109*, E02003, doi:10.1029/2003JE002172.

Li, Q., and W. S. Kiefer (2007), Mantle convection and magma production on present-day Mars: Effects of temperature-dependent rheology, *Geophys. Res. Lett.*, *34*, L16203, doi:10.1029/2007GL030544.

Lingenfelter, R. E., and G. Schubert (1973), Evidence for convection in planetary interiors from first-order topography, *Earth Moon Planets*, *7*(1), 172–180, doi:10.1007/BF00578814.

Marinova, M. M., O. Aharonson, and E. Asphaug (2008), Mega-impact formation of the Mars hemispheric dichotomy, *Nature*, *453*(7199), 1216–1219, doi:10.1038/nature07070.

Matsuyama, I., and M. Manga (2010), Mars without the equilibrium rotational figure, Tharsis, and the remnant rotational figure, *J. Geophys. Res.*, *115*, E12020, doi:10.1029/2010JE003686.

Matsuyama, I., J. X. Mitrovica, M. Manga, J. T. Perron, and M. A. Richards (2006), Rotational stability of dynamic planets with elastic lithospheres, *J. Geophys. Res.*, *111*, E02003, doi:10.1029/2005JE002447.

McGovern, P. J., S. C. Solomon, D. E. Smith, M. T. Zuber, M. Simons, M. A. Wieczorek, R. J. Phillips, G. A. Neumann, O. Aharonson, and J. W. Head (2002), Localized gravity/topography admittance and correlation spectra on Mars: Implications for regional and global evolution, *J. Geophys. Res.*, *107*(E12), 5136, doi:10.1029/2002JE001854.

McNamara, A. K., and S. Zhong (2004), Thermochemical structures within a spherical mantle: Superplumes or piles?, *J. Geophys. Res.*, *109*, B07402, doi:10.1029/2003JB002847.

McSween, H. Y., T. L. Grove, R. C. F. Lentz, J. C. Dann, A. H. Holzheid, L. R. Riciputi, and J. G. Ryan (2001), Geochemical evidence for magmatic water within Mars from pyroxenes in the Shergotty meteorite, *Nature*, *409*(6819), 487–490, doi:10.1038/35054011.

Médard, E., and T. L. Grove (2006), Early hydrous melting and degassing of the Martian interior, *J. Geophys. Res.*, *111*, E11003, doi:10.1029/2006JE002742.

Mège, D., and P. Masson (1996), A plume tectonics model for the Tharsis province, Mars, *Planet. Space Sci.*, *44*(12), 1499–1546, doi:10.1016/S0032-0633(96)00113-4.

Melosh, H. J. (1980), Tectonic patterns on a reoriented planet: Mars, *Icarus*, *44*(3), 745–751, doi:10.1016/0019-1035(80)90141-4.

Navrotsky, A. (1995), Thermodynamic properties of minerals, in *Mineral Physics and Crystallography: A Handbook of Physical Constants, AGU Ref. Shelf*, vol. 2, edited by T. J. Ahrens, pp. 18–28, AGU, Washington, D. C.

Neumann, G. A., M. T. Zuber, M. A. Wieczorek, P. J. McGovern, F. G. Lemoine, and D. E. Smith (2004), Crustal structure of Mars from gravity and topography, *J. Geophys. Res.*, *109*, E08002, doi:10.1029/2004JE002262.

Nimmo, F., and K. Tanaka (2005), Early crustal evolution of Mars, *Annu. Rev. Earth Planet. Sci.*, *33*(1), 133–161, doi:10.1146/annurev.earth.33.092203.122637.

Nimmo, F., S. D. Hart, D. G. Korycansky, and C. B. Agnor (2008), Implications of an impact origin for the Martian hemispheric dichotomy, *Nature*, *453*(7199), 1220–1223, doi:10.1038/nature07025.

Ogawa, M., and T. Yanagisawa (2011), Numerical models of Martian mantle evolution induced by magmatism and solid-state convection beneath stagnant lithosphere, *J. Geophys. Res.*, *116*, E08008, doi:10.1029/2010JE003777.

Parmentier, E. M., and M. T. Zuber (2007), Early evolution of Mars with mantle compositional stratification or hydrothermal crustal cooling, *J. Geophys. Res.*, *112*, E02007, doi:10.1029/2005JE002626.

Perron, J. T., J. X. Mitrovica, M. Manga, I. Matsuyama, and M. A. Richards (2007), Evidence for an ancient Martian ocean in the topography of deformed shorelines, *Nature*, *447*(7146), 840–843, doi:10.1038/nature05873.

Phillips, R. J., et al. (2001), Ancient geodynamics and global-scale hydrology on Mars, *Science*, *291*(5513), 2587–2591, doi:10.1126/science.1058701.

Pollack, H. N. (1986), Cratonization and thermal evolution of the mantle, *Earth Planet. Sci. Lett.*, *80*(1–2), 175–182, doi:10.1016/0012-821X(86)90031-2.

Reese, C. C., C. P. Orth, and V. S. Solomatov (2010), Impact origin for the Martian crustal dichotomy: Half emptied or half filled?, *J. Geophys. Res.*, *115*, E05004, doi:10.1029/2009JE003506.

Roberts, J. H., and S. Zhong (2006), Degree-1 convection in the Martian mantle and the origin of the hemispheric dichotomy, *J. Geophys. Res.*, *111*, E06013, doi:10.1029/2005JE002668.

Roberts, J. H., and S. Zhong (2007), The cause for the north–south orientation of the crustal dichotomy and the equatorial location of Tharsis on Mars, *Icarus*, *190*(1), 24–31, doi:10.1016/j.icarus.2007.03.002.

Sleep, N. H. (1994), Martian plate tectonics, *J. Geophys. Res.*, *99*(E3), 5639–5655, doi:10.1029/94JE00216.

Solomon, S. C., et al. (2005), New perspectives on ancient Mars, *Science*, *307*(5713), 1214–1220, doi:10.1126/science.1101812.

Šrámek, O., and S. Zhong (2010), Long-wavelength stagnant lid convection with hemispheric variation in lithospheric thickness: Link between Martian crustal dichotomy and Tharsis?, *J. Geophys. Res.*, *115*, E09010, doi:10.1029/2010JE003597.

Tanaka, K. L., D. H. Scott, and R. Greeley (1992), Global stratigraphy, in *Mars*, edited by H. H. Kieffer et al., chap. 11, pp. 345–382, Univ. of Ariz. Press, Tucson.

Wanke, H., and G. Dreibus (1994), Chemistry and accretion history of Mars [and discussion], *Philos. Trans. R. Soc. London, Ser. A*, *349*(1690), 285–293, doi:10.1098/rsta.1994.0132.

Wilhelms, D. E., and S. W. Squyres (1984), The Martian hemispheric dichotomy may be due to a giant impact, *Nature*, *309*(5964), 138–140, doi:10.1038/309138a0.

Willemann, R. J. (1984), Reorientation of planets with elastic lithospheres, *Icarus*, *60*(3), 701–709, doi:10.1016/0019-1035(84)90174-X.

Wise, D. U., M. P. Golombek, and G. E. McGill (1979), Tectonic evolution of Mars, *J. Geophys. Res.*, *84*(B14), 7934–7939, doi:10.1029/JB084iB14p07934.

Zhong, S. J. (2009), Migration of Tharsis volcanism on Mars caused by differential rotation of the lithosphere, *Nat. Geosci.*, *2*(1), 19–23, doi:10.1038/ngeo392.

Zhong, S. J. (2011), A critical assessment of models for Martian crustal dichotomy based on crustal production and re-distribution and crustal magnetization, *Lunar Planet. Sci.*, *XLII*, Abstract 2563.

Zhong, S. J., and M. T. Zuber (2001), Degree-1 mantle convection and the crustal dichotomy on Mars, *Earth Planet. Sci. Lett.*, *189*(1–2), 75–84, doi:10.1016/S0012-821X(01)00345-4.

Zhong, S. J., M. T. Zuber, L. Moresi, and M. Gurnis (2000), Role of temperature-dependent viscosity and surface plates in spherical shell models of mantle convection, *J. Geophys. Res.*, *105*(B5), 11,063–11,082, doi:10.1029/2000JB900003.

Zhong, S. J., A. McNamara, E. Tan, L. Moresi, and M. Gurnis (2008), A benchmark study on mantle convection in a 3-D spherical shell using CitcomS, *Geochem. Geophys. Geosyst.*, *9*, Q10017, doi:10.1029/2008GC002048.

O. Šrámek and S. Zhong, Department of Physics, University of Colorado at Boulder, 390 UCB, Boulder, CO 80309-0390, USA. (ondrej.sramek@colorado.edu)